Nanoscale Horizons

ROYAL SOCIETY OF CHEMISTRY

COMMUNICATION

View Article Online
View Journal | View Issue

Cite this: *Nanoscale Horiz.*, 2023, 8, 1243

Received 29th May 2023,
Accepted 10th July 2023

DOI: 10.1039/d3nh00203a

rsc.li/nanoscale-horizons

A nanofluidic sensing platform based on robust and flexible graphene oxide/chitosan nanochannel membranes for glucose and urea detection†

Kou Yang,[ab] Qinyue Wang,[ac] Kostya S. Novoselov[ab] and Daria V. Andreeva *[ab]

We present the development of a health-monitoring nanofluidic membrane utilizing biocompatible and biodegradable graphene oxide, chitosan, and graphene quantum dots. The nanoconfinement provided by graphene oxide nanolayers encapsulates chitosan molecules, allowing for their conformational changes and switchable hydrophobic–hydrophilic behavior in response to pH variations. This low-dimensional membrane operates as an array of nanofluidic channels that can release quantum dots upon pH change. The photoluminescence emission from quantum dots enables rapid and reliable optical visualization of pH changes, facilitating efficient human health monitoring. To ensure fouling prevention and enable multiple usages, we adopt a design approach that avoids direct contact between biomarkers and the nanochannels. This design strategy, coupled with good mechanical properties (Young's modulus of 5.5 ± 0.7 GPa), preserves the integrity and functionality of the sensors for repeated sensing cycles. Furthermore, leveraging the memory effect, our sensors can be reloaded with graphene quantum dots multiple times without significant loss of selectivity, achieving reusability. The wide-ranging capabilities of 2D materials and stimuli-responsive polymers empower our sustainable approach to designing low-dimensional, robust, and flexible sensing materials. This approach allows for the integration of various biorecognition elements and signal transduction modes, expanding the versatility and applications of the designed materials.

New concepts

We propose a novel concept in the development of health-monitoring technology utilizing a nanofluidic membrane composed of biocompatible and biodegradable materials, including graphene oxide, chitosan, and graphene quantum dots. In general, micro- and nanofluidic-based devices offer advantages like precise control over analyte flow, efficient mixing, reduced sample and reagent consumption, and integration with sensors or other analytical tools. However, the fabrication of nanofluidic devices as well as microfluidic devices is complex and requires time-consuming multistage lithography techniques, template-assisted methods and nanopatterning. In this study, we design a novel nanofluidic biodetection platform based on self-assembly. Self-assembly is a rapid and energy-saving method for assembling nanocompartment materials. This design strategy, combined with the membrane's favorable mechanical properties (Young's modulus of 4.5 GPa), preserves the integrity and functionality of the sensors for repeated sensing cycles. The membrane functions as an array of nanofluidic channels that can release graphene quantum dots upon changes in pH. The photoluminescence emission from these quantum dots allows for rapid and reliable optical visualization of pH changes, facilitating efficient monitoring of human health indicators. Furthermore, our sensors exhibit a memory effect, enabling multiple reloads of graphene quantum dots without significant loss of selectivity, achieving enhanced reusability. This feature contributes to the sustainability of our approach. By leveraging the capabilities of two-dimensional materials and stimuli-responsive polymers, we have developed a sustainable approach to designing low-dimensional, robust, and flexible sensing materials. This approach enables the integration of various biorecognition elements and signal transduction modes, expanding the versatility and applications of the designed materials.

Diabetes and liver diseases, common in daily life, remain challenging for the global health system.[1–4] Despite the commercial continuous glucose monitoring system (CGMS) and urea monitoring devices, better materials and designs are under investigation to overcome the present deficiencies. Biosensors are widely employed as an analytical strategy,[5] owing to their high sensitivity, rapid response and real-time measurements.[6,7]

While various materials have shown commercial prospects in glucose and urea detection, some of the designs need serum, which does not consider the danger of infection with diseases like acquired immune deficiency syndrome (AIDS). In recent years, nanocomposites like ZnO@rGO, NiO–MoO_3 and Ag/NiOOH have been verified to have promising potential in urea/glucose detection.[8–10] These materials enable the design of non-enzymatic

[a] *Department of Materials Science and Engineering, National University of Singapore, 117575, Singapore. E-mail: daria@nus.edu.sg*
[b] *Institute for Functional Intelligent Materials, National University of Singapore, 117544, Singapore*
[c] *School of Materials Science and Engineering, Northwestern Polytechnical University, 710072, Shaanxi, China*

† Electronic supplementary information (ESI) available. See DOI: https://doi.org/10.1039/d3nh00203a

sensors, which depend on the high electrochemical activity of nanocomposite electrodes.[11,12] However, such sensors often cannot be reused. Moreover, these biosensors are often only suitable for monitoring a specific substance, which has limitations in the commercial field.

Integrating microfluidics or nanofluidics with sensors offers several advantages, including improved sensitivity, multiple sensing cycles, reduced sample and reagent consumption, and the ability to perform complex assays or analyses in a compact and portable format.[13,14] Microfluidics and nanofluidics deal with fluidic systems at the micro/nanoscale, with channels and structures typically on the order of micro or even nanometers.[15] Nanofluidic sensors have applications in areas such as DNA sequencing,[16] single-molecule sensing,[17] and single-cell analysis.[18] The advantages include enhanced sensitivity, small volume, fast response and reusability.

In general, micro- and nanofluidic-based devices offer advantages like precise control over analyte flow, efficient mixing, reduced sample and reagent consumption, and integration with sensors or other analytical tools. However, the fabrication of nanofluidic devices as well as microfluidic devices is complex and requires time-consuming multistage lithography techniques, template-assisted methods and nanopatterning.

In this study, we design a novel nanofluidic biodetection platform based on the self-assembly of graphene oxide (GO), chitosan (CS) and graphene quantum dots (GQDs). Self-assembly is a rapid and energy-saving method for assembling nanocompartment materials. This approach harnesses the inherent properties of the materials themselves to spontaneously organize and form complex structures or compartments without the need for external energy inputs or complicated assembly processes. In our nanofluidic GO/GQDs/CS (GGC) membranes, CS molecules are encapsulated in GO nanocompartments and form nanochannels that switch hydrophilic/hydrophobic states in response to pH. As part of a sensor device, the membrane operates as an array of nanofluidic channels.

Through the self-assembly of biocompatible and biodegradable materials, we strive to create products and implement processes that align with the principles of sustainability. First, emerging biosensors[19,20] are explored by integrating biodegradable and biocompatible two-dimensional graphene-based materials into the polymer matrix.[21] In particular, due to the high specific area,[22] hydrophilicity[23] and biocompatibility,[24,25] GO is considered as a new material for miniature biosensors with high selectivity.[26–28] Apart from GO, CS extracted from natural sources has also shown promising potential in biosensing applications.[29] Owing to the pH-sensitivity, the hydrophilic/hydrophobic properties of CS switch in response to pH change.[30–32] Among other pH-sensitive hydrogels, chitosan has a faster rate of responsiveness.[33] As a biocompatible nanomaterial, GQDs have excellent optical properties, including strong fluorescence, high quantum yield, and broad absorption. These features make them suitable for optical sensors, such as fluorescence sensors, biosensors, and chemosensors.[34–36]

The ability of the GGC membrane to respond to pH changes induced by biochemical processes opens possibilities for the development of sensors for detecting the analytes in aqueous solutions and avoiding direct contact with biomarkers. By monitoring the changes in pH and PL intensity, biomarkers and enzymes are not directly in contact with the sensor surface. Thus, we avoid contamination or fouling[38] that can occur during tests and can use our membrane for multiple uses. At acidic pH, the nanochannels are in a hydrophilic state and the membrane can be impregnated with an aqueous GQD dispersion. At neutral/basic pH, the nanochannels are in a hydrophobic state and pump the aqueous GQD dispersion out of the membrane. Thus, we can optically detect the pH change that accompanies such biochemical reactions as glucose or urea oxidation. The working pH range is around 4.6 (pK_a value of GO) and 6.5 (pK_a value of chitosan[37]); therefore, our sensors are highly sensitive to even a small pH shift from the physiological pH range and highly sensitive to variations in biomarkers' concentrations.

The use of the nanofluidic GGC membrane as a pH-responsive sensing platform offers potential advantages such as simplicity, sensitivity, and real-time monitoring capabilities. To this end, we calibrate our membranes with varying concentrations of urea and glucose. Indeed, our nanofluidic membranes can detect up to several millimolar (mM) concentrations of glucose, which is relatively high sensitivity.[39,40] However, further research and validation would be necessary to explore the practical viability and performance of this sensor in different applications.[40]

Importantly, we develop a membrane with an array of nanofluidic channels that is easy to assemble and has outstanding mechanical properties. Young's modulus is 5.5 $\pm$ 0.7 GPa for the GGC membrane, even higher than the pristine GO membrane (4 GPa). Additionally, all components, GO, GQDs and chitosan are biocompatible and biodegradable, making the platform sustainable due to its reusability, flexibility, compactness, and robustness.

We prepare the pH-responsive GGC membranes by a vacuum-assisted self-assembly method (Fig. S1, ESI†). Briefly, a controlled amount of GQDs is first added to the dispersion of GO to form a GO/GQDs mixture, and then a self-assembly approach is employed by physical blending to entrap CS macromolecules (chitosan powder with M_w $\sim$ 190–375 kDa dissolved in 1 vol%/vol acetic acid) into the GO/GQDs channels. By increasing the amount of GO, GQDs and CS, a soft free-standing GGC membrane can be easily prepared (see Methods for details). Owing to the opposite charges of functional groups of GO and CS and the van der Waals interactions between GO nanolayers, GO with CS is assembled into a Layer-by-Layer (LbL) structure during vacuum filtration. Zeta potential measurements (Fig. S2, ESI†) show that the dispersion of GO flakes is stable in the whole pH range. A zeta potential value below -30 mV indicates its colloidal stability. For pure CS and GO/CS mixtures, the value of the zeta potential dropped to 0 when the pH is $\geq$6. At a pH value above the pK_a value of CS, the hydrophobic and uncharged CS becomes insoluble in water, leading to the aggregation of CS and phase separation. Thus, the optimal pH range for the self-assembly is around 3.

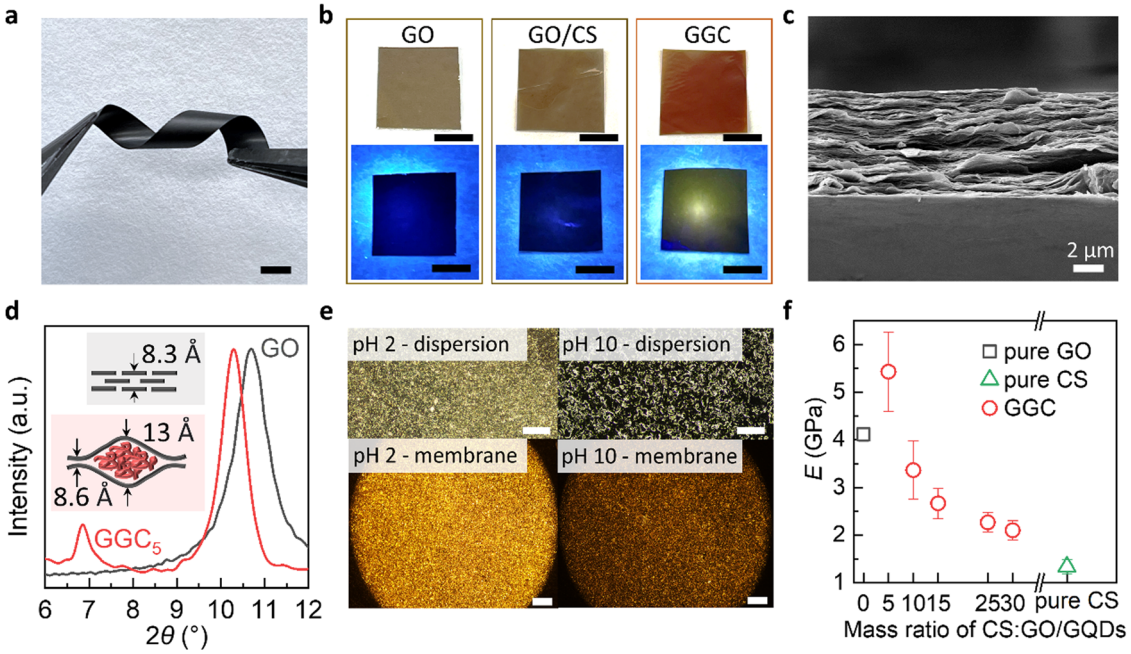

Fig. 1 Preparation and characterization of GGC membranes. (a) Digital photo of a robust and flexible GGC membrane strip twisted by tweezers. Scale bar: 1 cm. (b) Digital photos of GO, GO/CS and the GGC membrane under natural light (top) and 365 nm UV light (bottom). Membrane size: 1 cm × 1 cm. Scale bar: 5 mm. (c) Cross-section SEM image of a free-standing GGC_5 membrane. (d) X-ray diffraction (XRD) spectra of the pristine GO and GGC_5 membrane. (e) Optical polarizing images of the reversible phase transition of the GGC dispersion (top) and GGC membrane (bottom) in response to pH. Scale bar: dispersion −200 μm, membrane −500 μm. (f) Young's modulus of pure GO, pure CS and GGC membranes as a function of the mass ratio of CS to GO/GQDs.

The thickness of the membranes can be controlled by adjusting the amount of GO and CS used in their preparation. Increasing the concentration of GO and CS results in μm-thick free-standing membranes, while decreasing the concentration leads to nm-thin supported membranes. As we see in Fig. 1a, a free-standing GGC membrane is robust and flexible. The ability to tune the membrane thickness enables the assembly of membranes for the creation of nanofluidic devices. This flexibility in controlling the thickness of the membrane facilitates the design and fabrication of the arrays of nanoscale channels, allowing for precise manipulation and transport of fluids at the nanoscale.

According to the used mass ratio of CS to GO/GQDs, we assigned the membranes as GGC_5, GGC_{10}, GGC_{15}, GGC_{25}, and GGC_{30}. Note, that an insufficient loading of CS leads to the aggregation of GO into flocculent precipitates. Also, when the mass ratio of GO to GQDs is less than 1, the PL of the GQDs is quenched. Through optimization, the mixing ratio of CS, GO, and GQDs is determined to be 5 : 0.2 : 0.8. Under natural light, the membrane exhibits a brownish-yellow color, while under UV light, it emits a yellowish light, as depicted in Fig. 1b. In contrast, the pure GO membrane or GO/CS membrane does not exhibit any detectable PL.

The GGC membrane exhibits a characteristic lamellar morphology resembling GO paper, as observed in the scanning electron microscopy (SEM) image of the cross-sections (Fig. 1c). In the X-ray diffraction (XRD) spectra of the composite membranes (Fig. 1d), two distinct peaks are observed, indicating the presence of two interlayer distances within the GGC membranes. The interlayer spacing (d) of the nanochannels formed by chitosan encapsulated between the GO laminates measures 13 Å, whereas the region without CS exhibits an interlayer spacing of 8.6 Å. This structural arrangement suggests the presence of nanochannels within the membrane structure, where CS molecules are enclosed between the layers of GO.

Our study reveals a phenomenon where CS within the GO nanochannels exhibits a reversible switch between hydrophilic and hydrophobic states in response to changes in pH. The transition between the hydrophobic collapsed and hydrophilic expanded states of CS coils in the GO nanochannels leads to different optical properties, as illustrated in Fig. 1e. At pH 10, the hydrophobic intramolecular interactions in the CS fraction are dominant, and CS molecules are partially reoriented in ordered hydrophobic domains. The birefringence of the materials at pH 2 might be explained by the formation of ordered anisotropic materials stabilized by the hydrophilic interactions of GO and CS.

The pH-responsive reorientation and alignment of CS molecules are not only linked to changes in hydrophilicity/hydrophobicity but are also associated with the uptake and release of water molecules. Within the GO nanochannels, the interplay between the GO nanolayers and water molecules establishes a distinctive 2D liquid-like environment, facilitating the entrapment of GQDs. Notably, as CS undergoes a transition to a hydrophobic state, the reorientation of the hydrophobic domains induces stresses and strains within the system.

These mechanical perturbations have the potential to trigger the expulsion of water molecules and GQDs out of the nanochannels, thereby influencing the overall transport properties of the nanofluidic membrane.

As shown in Fig. 1f, the self-assembled composite membranes exhibit high tensile strength. We compared Young's modulus and the ultimate tensile strength for GGC membranes with different CS concentrations. For control purposes, we also prepared a pristine GO membrane and CS membrane. With the increase in CS concentration, Young's modulus of the GGC membrane decreased and the strain increased. The significant improvement in the tensile strength of the GGC composite might be due to cross-linking between the GO nanolayers and CS macromolecules. The Young's modulus of the GGC_5 membrane is measured to be 5.5 ± 0.7 GPa, which is higher than that of the pristine GO membrane, which has a Young's modulus of 4 GPa. Additionally, this value is several orders greater than those measured for the polymeric hydrogels (450–490 kPa).[23] In particular, the self-assembled GGC composites can form robust large-scale membranes (Fig. S3, ESI†) for the integration and patterning of flexible devices.

Using quartz crystal microbalance (QCM) and permeability tests, we monitor the water absorption capacity of GGC membranes and water transport through the nanochannels *vs.* pH. The 0.1 mg GGC membrane (approx. thickness is 450 nm) can reach the swelling equilibrium within 30 seconds in any pH water environment (Fig. S4, ESI†). Among other pH-sensitive polymeric hydrogels, CS has a faster rate of responsiveness, which can be attributed to its super hydrophilicity and favorable permeability of water.[33]

The swelling capacity (Fig. 2a) is derived from fitting the swelling curves by a Voigt model (Fig. S4, ESI†). We see that the swelling curves can be accurately fitted by a Voigt model, which suggests that the material's swelling behavior may be fully described by the combined elastic and viscous deformations assumed by the model for polymeric hydrogels. The result indicates that the degree of swelling drops sharply at pH > 6 due to an increase in the degree of cross-linking of unchanged CS macromolecules. Notably, the excellent reversibility of the swelling capacities between pH 3 and pH 7 was revealed by cyclic QCM measurements (Fig. 2b). Significant mass increases/decreases were found when the external environment alternated between pH 3 and pH 7 (Fig. S6, ESI†). This reversibility was observed within the biosensing pH range relevant to glucose and urea detection, which will be further discussed in the subsequent sections.

As expected, the permeability experiments (Fig. 2a) show that the water flux through the nanochannels in GGC membranes also depends on pH. At pH ≥ 5, the nanochannels are hydrophobic and are closed to water. At pH < 5 the nanochannels are hydrophilic and transfer water. For the pristine GO membrane, no significant changes in terms of water

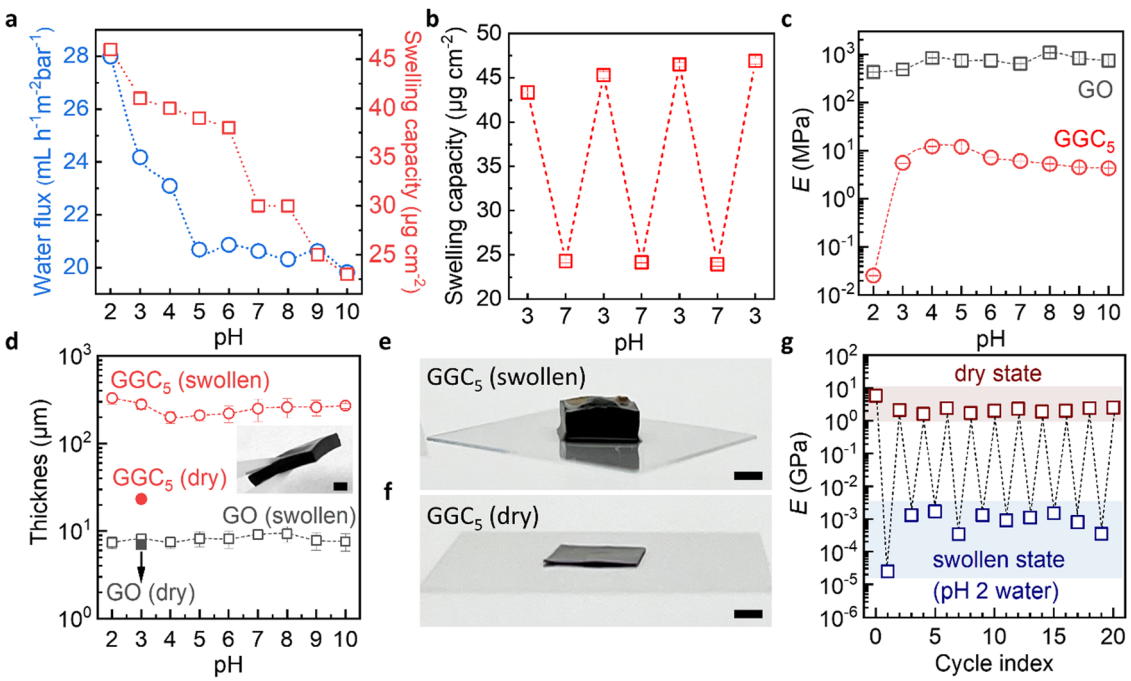

Fig. 2 pH-responsive swelling of GGC membranes. (a) Water permeability and swelling capacity of the GGC_5 membrane as a function of water pH. (b) Swelling capacity change of a single GGC_5 membrane in a continuous cyclic QCM test, with the pH of the feed water cycled between 3 and 7. (c) Young's modulus of GO and the GGC_5 membrane in water as a function of pH. Soaking time: 10 min. (d) Thickness of a 5 mg GO and a GGC_5 (with 5 mg GO) membrane in the dry and swollen state (immersed in DI water with different pH for 10 min). Inset: a digital photo of a robust GGC membrane after swelling in DI-water for 2 h, scale bar: 2 mm. (e and f) Digital pictures showing a GGC_5 (with 5 mg GO) membrane in a dry state (f) and after immersing in pH 2 water for 2 h (e), scale bar: 2 mm. (g) Young's modulus of GGC_5 membranes cycling between dry and swollen states. The swollen state is tested after immersing the membrane in pH 2 water for 10 min.

uptake/permeability are observed when the pH is altered (Fig. S5, ESI†). Thus, the material exhibits two interconnected functional properties that work in tandem to facilitate the transport properties of the nanofluidic channels. These properties involve the reorientation of CS domains and the movement of water.

The performance of biosensors depends not only on the specificity and sensitivity of the biological recognition element, but also on the mechanical properties of the device in the presence of biological fluids. The mechanical properties of swollen materials that can adsorb large amounts of water can present challenges for applications.

We see that even filled with water, our membranes exhibit exceptional mechanical properties. To measure the mechanical properties of membranes, we prepared a GO membrane and GGC membrane using the same amount of GO (5 mg). The thickness of the dry GO membrane was measured to be 7 ± 0.5 μm, while the thickness of the dry GGC membrane was 20 ± 2 μm. The membranes were immersed in solutions with varying pH levels for a duration of 10 minutes. Following this, we measured the thicknesses of the membranes, obtained stress–strain curves and calculated Young's modulus in the swollen states.

Young's modulus of the pure GO membranes is approx. 1 ± 0.5 GPa in the swollen state in the whole pH range (Fig. 2c). The thicknesses of such membranes macroscopically also did not change (Fig. 2d) due to the limited water absorption by the pure GO membrane during the experimental time. In contrast, Young's modulus of the GGC drops to approx. 15 ± 5 MPa in the pH range from 3 to 10, which is still an order of magnitude higher than that of typical hydrogels. Typical hydrogels with a crosslinking density of 2% can have a Young's modulus of about 1 MPa in the swollen state.[41] At pH 2, the Young's modulus of the GGC decreases to 20 kPa (Fig. S7, ESI†), which is a Young's modulus previously measured for hydrogels with a crosslinking density of 10%.[42] Due to the large swelling capacity of water, the thickness of GGC increases from 20 ± 2 μm to 200 ± 70 μm (Fig. 2d).

It is important to thoroughly characterize the robustness and reusability of our membranes under the specific conditions that are relevant to our intended applications. This involves conducting experiments and tests that simulate the expected usage and conditions of the membranes to evaluate their durability and ability to withstand repeated use. Therefore, we conducted long-term swelling testing by increasing the immersion time to 2 hours, which resulted in a significant increase in the thickness of our GGC composite membranes up to 2 mm (as shown in Fig. 2e and f). Despite this increase in thickness, our GGC composite membranes remained robust and stable and are easily handled even in a highly swollen state (inset in Fig. 2d). To evaluate the robustness and reusability of our GGC membranes, we tested Young's modulus of the membranes in both dry and swollen states under pH 2 conditions for 20 cycles (Fig. 2g). Our results show that when the membrane returns from the swollen state to the dry state, its mechanical properties recover to the original GPa level. This indicates that our GGC membrane exhibits superior stability for at least 20 cycles. Additionally, the mechanical properties of the GGC membrane can be controlled by manipulating environmental factors, such as humidity and pH conditions.

In the subsequent phase of our research, we proceeded to evaluate the performance of our membranes in monitoring actual biochemical processes that give rise to pH variations. Specifically, we focused on the oxidation of urea and glucose, which are known to induce pH changes. The sketch of an optical sensor with an integrated membrane is illustrated in Fig. 3, providing insights into the capability of our nanofluidic membranes to detect and track such biochemical processes.

The oxidation of urea results in the release of OH^- in the presence of urease, which increases the pH of the surrounding environment and induces the release of GQDs from our membranes. On the other hand, the oxidation of glucose by glucose oxidase (GO_x) leads to the formation of gluconic acid, which causes the pH of the environment to drop and allows the released GQDs to be reabsorbed by our membranes. These dynamic processes can be monitored and quantified by measuring the changes in the PL intensity of the released GQDs, which we use to develop a biosensor for urea and glucose detection.

We accurately detected the release of GQDs by performing PL measurements of aqueous solutions above the membranes. As demonstrated in Fig. 3b, the PL spectrum obtained at pH above 6.5 shows a strong peak at 525 nm due to the release of water and GQDs from the hydrophobic nanochannels. In contrast, the PL intensity at pH 2 is very low. Probably because at this pH GQDs are not released from the nanochannels and their diffusion is limited due to the charge and complexity of the nanochannel network. The linear dependence of PL intensity on pH enables us to monitor biochemical processes accompanied by pH changes (Fig. 3c).

During immersion in urea solution, the pH value changes from 3 to 7 (Fig. 4a–c). The increase in pH results in the release of GQDs from the nanochannels. The PL intensity exhibits a linear response to increasing urea concentration within the range of 50 μM to 200 μM, which is shown in the inset of Fig. 4a–c. 1.5 mM urea concentration refers to the highest concentration of urea that can be reliably detected by our sensing system.

The results obtained from our study demonstrate the sensitivity of the GGC membrane toward urea detection in the micromolar concentration range. The membrane exhibits a linear response range that extends down to a concentration of 50 μM. This means that the membrane is capable of accurately detecting and quantifying urea concentrations as low as 50 μM with a reliable and proportional response.

In biological and clinical applications, urea concentrations in bodily fluids like blood or urine can range from a few micromolar to millimolar levels. For certain applications, such as monitoring urea levels in patients with kidney disease or studying urea metabolism, a higher sensitivity might be desired.[43,44] A limit of detection of 50 μM for urea could be

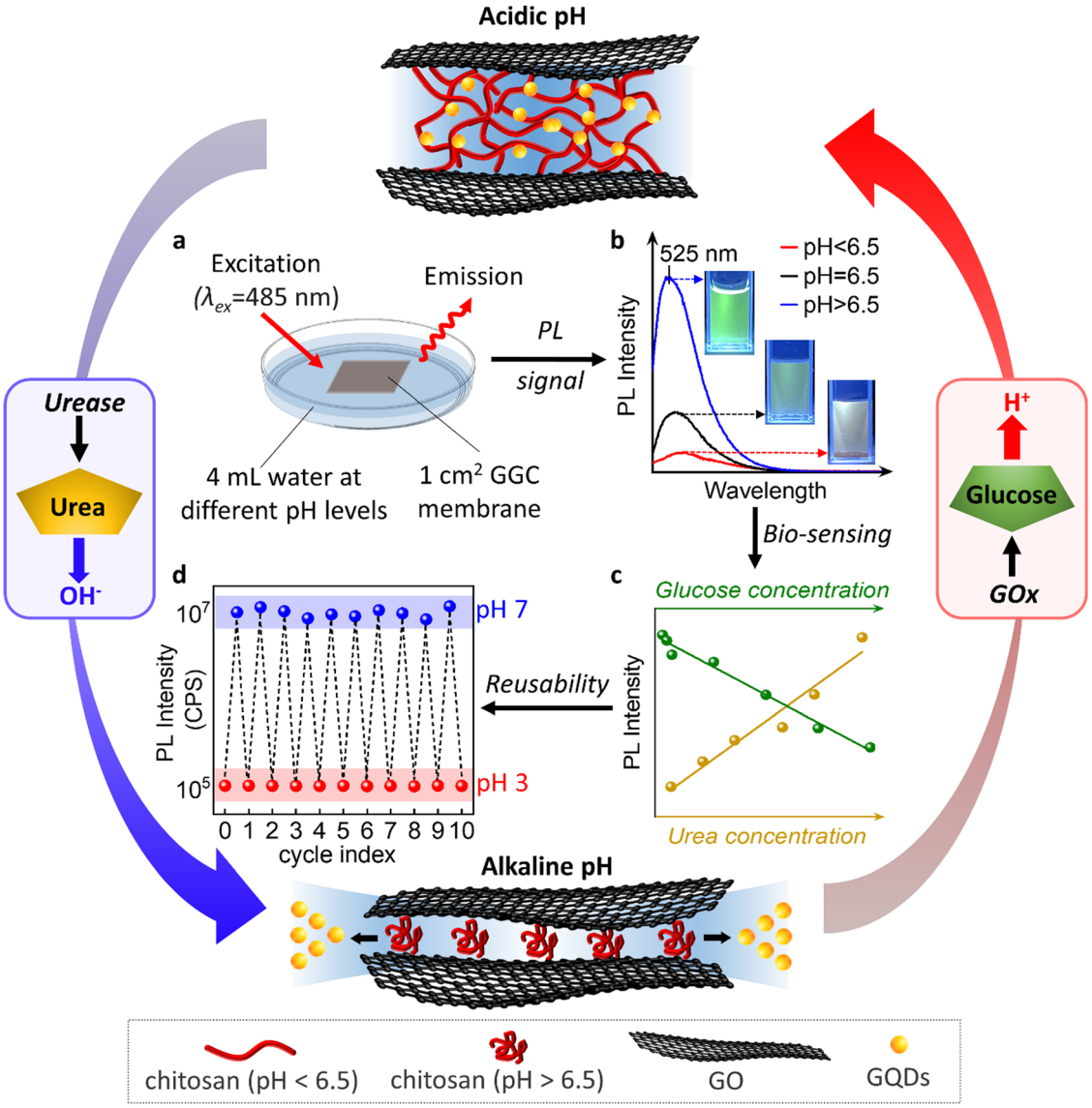

Fig. 3 pH-responsive GGC membrane as a reusable biosensor for urea/glucose detection. (a) Schematic illustration of the fluorescence sensor. (b) PL spectra of the water at different pH levels soaked with GGC membrane for 2 h. (c) The change of PL intensity depends on the concentration of glucose or urea. (d) Cyclic PL measurement showing the reusability of our nanofluidic device. The nanochannels can be reloaded with GQDs by the immersion of the device for 2 h in aqueous solution of GQDs. We repeated the recovery process 10 times after exposing devices for 15 min at pH 7.

considered good sensitivity in the field of environmental monitoring or water quality assessment.

In the case of glucose, we observe that as the concentration of glucose increases, the pH value of the solution decreased from 7 to 3 (Fig. 4d–f). This is due to the oxidation of glucose by glucose oxidase, which produces hydrogen ions and causes a decrease in pH. We observe a decrease in the PL intensity of the solution as the concentration of glucose increases (Fig. 4f). The slowing down of GQD release at acidic pH is the underlying cause of this phenomenon.

During the immersion in a glucose solution, we conducted experiments in the concentration range of 0.01 mM to 30 mM and observed that the intensity of the PL spectra monotonously decreased with the increase in glucose concentration (Fig. 4e and f). A linear relationship is observed between concentrations ranging from 0.01 mM to 2 mM, as depicted in the inserted figure in Fig. 4e and f. This finding demonstrates the sensitivity of our graphene-based glucose sensor for detecting glucose in millimolar concentrations.

This is particularly noteworthy as the glucose concentration in saliva, sweat, or tears is usually lower than 0.5 mM, making it difficult to detect non-invasively.[44] Our results suggest that our GGC membranes can offer a non-invasive approach to the diagnosis of glucose in these bodily fluids. Drawing blood for glucose testing can cause trauma to the human body, and our GGC glucose detection platform provides a promising alternative.

The sustainability of sensors also encompasses their reusability. In our study, we assessed the reusability of the sensor

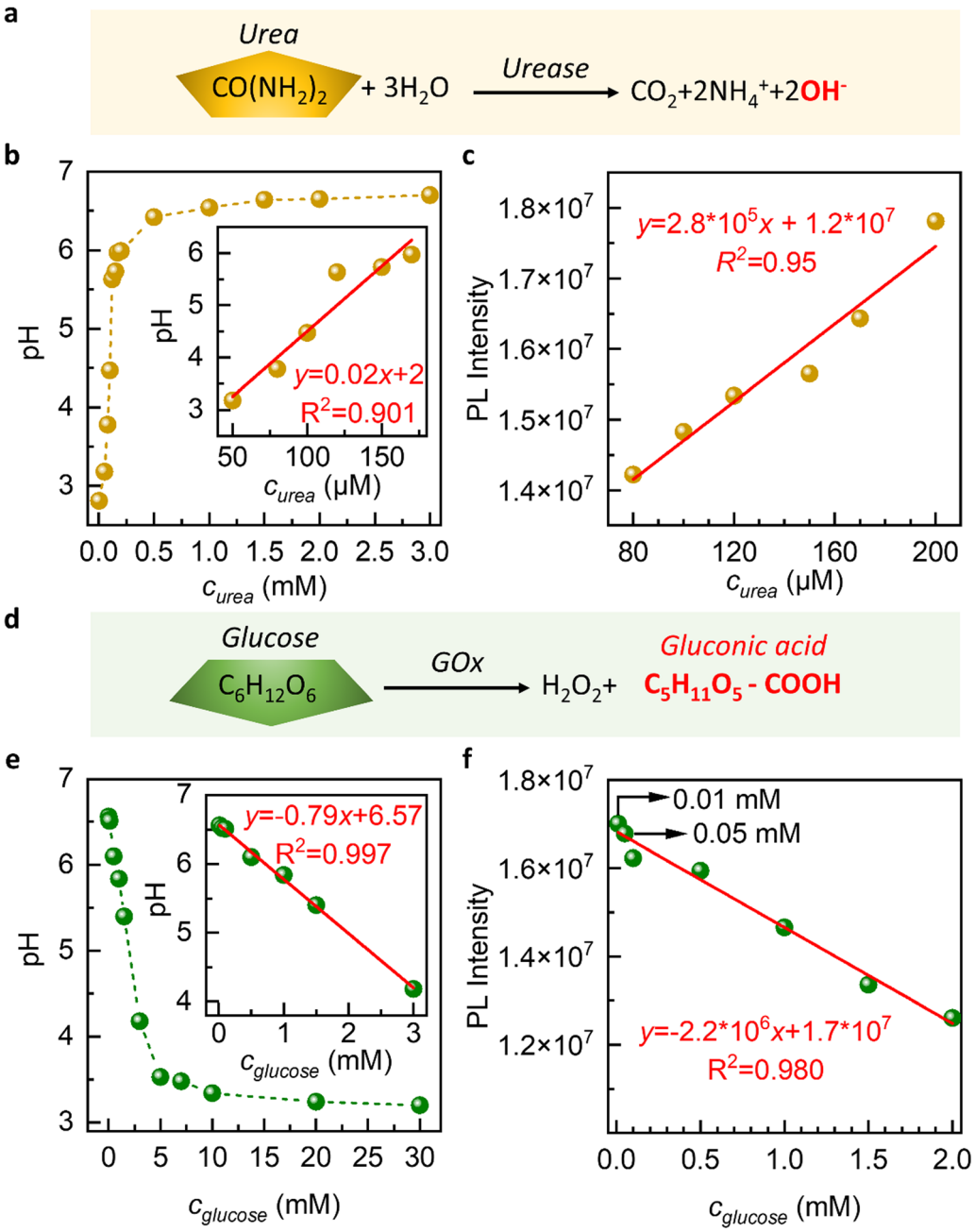

Fig. 4 Urea and glucose detection through the GGC membrane. (a) Illustration of the reaction between urea and urease. (b and c) pH (b) and PL intensity (c) of urea as a function of urea concentration. Urea at various concentrations was catalyzed by saturated urease. Inset: the linear relationship between pH (b-inset)/PL intensity (c-inset) and urea concentration and its fitting curves and parameters. (d) Illustration of the reaction between glucose and GO_x. (e and f) pH (e) and PL intensity (f) of glucose as a function of glucose concentration. Glucose at various concentrations was catalyzed by saturated GO_x. Inset: the linear relationship between pH (e-inset)/PL intensity (f-inset) and glucose concentration and its fitting curves and parameters.

through cyclic PL measurements, as shown in Fig. 3d. We found that the device maintains its integrity and performance even after undergoing 10 cycles, which represents the maximum number of cycles examined in this study.

During each cycle, the device is exposed to a pH 7 solution for 15 min followed by a pH 3 solution for 2 h. At pH 7, the nanochannels release GQDs within 15 min, leading to an increase in the PL of the external solution. Subsequently, at pH 3, we can reload the nanochannels with GQDs, a process that takes 2 h, resulting in a decrease in the PL of the external solution.

Notably, our device exhibits a distinct "memory effect". When the GQDs are encapsulated within the membrane at pH 3, they can be released into the surrounding environment at pH 7. Upon re-exposure to pH 3, the released GQDs re-enter the nanochannels and return to their original positions. However, if we initially utilize our materials at pH 7, the release of GQDs is not reversible. This suggests that the reloading process is

specific to the conditions in which the GQDs are initially encapsulated within the nanochannels at pH 3. This "memory effect" refers to the phenomenon where our nanochannels retain or "remember" a capacity or affinity for the entrapment of GQDs. The sensors with a memory effect can be reused or reloaded with the initial concentration of GQDs. The memory effect allows the sensor to recover its initial sensitivity upon regeneration.

In summary, our study successfully fabricated novel nanofluidic membranes for pH-responsive health monitoring through the self-assembly of CS, GO, and GQDs. Of significant importance is the development of a membrane featuring an array of nanofluidic channels that offers simplicity in assembly and exhibits exceptional mechanical properties.

Furthermore, the biocompatibility and biodegradability of all the components involved, including GO, GQDs, and CS, further contribute to the sustainability of the platform. The membrane's reusability, flexibility and compactness make it an attractive choice for biomedical applications. Our findings demonstrate that the sensor maintains its integrity and performance over multiple cycles of exposure to pH 7 and pH 3 solutions. The reversibility of GQD release is dependent on the initial pH conditions. The nanochannels prepared at pH 3 release GQDs at pH 7 and can be reloaded with GQDs at pH 3, exhibiting a distinct "memory effect". The nanofluidic sensing platform with a memory effect can be reused multiple times without significant loss of selectivity.

The combination of these characteristics positions our nanofluidic membrane as a promising solution, offering a multitude of potential benefits. With its easy assembly, good mechanical properties, biocompatibility, biodegradability, and sustainability, the membrane serves as a platform for its broad application in healthcare, diagnostics, biotechnologies, and environmental technologies. Moreover, these remarkable features open new avenues for innovative applications in the future, ensuring the membrane's significant impact and contribution to various industries.

Experimental Section

Materials

Aqueous graphene oxide dispersion (GO, 4 mg mL^{-1}, monolayer content $>95\%$, Graphenea Inc., USA), chitosan (CS, $M_w \sim$ 190–375 kDa, powder, from shrimp shells, Sigma-Aldrich), polyethersulfone membrane filter (PES, 0.03 μm, 47 mm, Sterlitech Corporation, USA), Anodisc 47™ filter (pore size −0.02 μm, diameter 47 mm, Whatman, USA), acetic acid (HOAc, glacial, ReagentPlus®, ≥99%, Sigma-Aldrich), graphene quantum dots (GQDs, aqua green luminescent, 1 mg mL^{-1}, Sigma-Aldrich), hydrochloric acid (HCl, ACS reagent, 37%, Sigma-Aldrich), and sodium hydroxide solution (NaOH, 50% in H_2O, Sigma-Aldrich) were used. All materials were received and used without further purification.

Membrane preparation

CS/HOAc dispersion (5 mg mL^{-1}) was obtained by dissolving chitosan (2 g) in HOAc (1 vol%/vol, 400 mL) upon magnetic stirring for 24 h at room temperature. The original aqueous graphene oxide dispersion (4 mg mL^{-1}, 20 mL) was added into deionized water (380 mL) to obtain diluted GO dispersion (0.2 mg mL^{-1}). To get a homogeneous GO/GQDs dispersion, the prepared GO and GQDs dispersion was mixed with a mass ratio of 1 : 1. Then, CS/HOAc dispersion was mixed with GO/GQDs dispersion with a mass ratio from 5 to 30, and the colloids were then mixed for 10 minutes by a shaker (rotation speed – 500 rpm, Vortex Mixer, USA). GGC composite membranes were prepared by vacuum filtration of the aforesaid mixture through two types of membrane filters: Anodisc™ 47 and polyethersulfone membrane. Vacuum filtration was maintained for 24 h, and the obtained membrane was then dried overnight in a dry cabinet at room temperature. The resulting membranes were named GGC_x, where x is the mass ratio of chitosan to GO/GQDs. For comparison, a pristine GO membrane and chitosan membrane can be easily prepared with the same approach.

Characterization methods

X-Ray diffraction (XRD) was carried out on Bruker D8 ADVANCE with a Cu Kα tube radiation source (1.5418 Å) in a step of 0.02° per second from 2° to 20°. The membrane thickness was measured by an Alpha-Step IQ Surface Profiler (KLA Tencor). The mechanical properties were measured using a Dynamic Mechanical Analyser (DMA 850, TA Instruments). Scanning electron microscopy (SEM) images were obtained by a ZEISS Sigma 300 FE SEM system. The membrane samples were sputtered with 5 nm gold before observation. Quartz-Crystal Microbalance (QCM) measurements were performed by the QSense Explorer System (QE 401 Electronic Unit, QCP 101 Chamber Platform, QFM 401 Flow Module). A 5 MHz Au electrode was used with the pump speed of 30 μL min^{-1}.

Setup for water permeation experiments

Water and permeation experiments were performed using a set of side-by-side diffusion cells (Yuyan Instruments, Shanghai) with a membrane fixed between two cell compartments, *e.g.* the feed compartment and the drain compartment. The feed compartment was filled with DI water (20 mL) at different pH, while the drain compartment was sucrose (20 mL, 2.5 mol L^{-1}) to induce the osmotic pressure between two cell compartments. The pH of DI water is controlled by the addition of a certain volume of HCl or NaOH. After 24 h of permeation, the weight of the sucrose solution was recorded to calculate the water flux.

Urea and glucose detection using GGC membranes

1 M aqueous urea, prepared with urea powder and phosphate buffer saline (pH = 3), is diluted into various concentrations. According to the optimization experiments we operated, the amounts of urease and urea show a linear relationship (for example: for 200 μM urea, 400 U urease is needed) in the range of 1 μM–3 mM. 10 mL dilute urea solution was reacted with the corresponding amount of urease for 10 min at 37 °C. Subsequent experiments were based on the different pH solutions to obtain different PL intensities. Similar to urea detection,

dilute glucose solution, GO_x and phosphate buffer saline (pH = 6) are used for the reaction. The linear relationship for the glucose and GO_x is that every 1 mM glucose needs 1000 U GO_x, ranging from 100 μM to 10 mM. The experiments are operated for 60 min at 37 °C. Since GO_x itself shows yellow color, the final PL intensity should offset the initial ones.

Author contributions

D. V. A. and K. S. N. designed the experiments and supervised the project. K. Y., Q. W. performed the experiments, solved the technical issues, and checked the experimental results. K. Y., Q. W., D. V. A. and K. S. N. co-wrote the paper. All authors discussed the results and commented on the manuscript.

Conflicts of interest

The authors declare no competing interests.

Acknowledgements

This research is supported by the Ministry of Education, Singapore, under its Research Centre of Excellence award to the Institute for Functional Intelligent Materials (I-FIM, project no. EDUNC-33-18-279-V12).

References

1 R. Gallego-Durán, J. Ampuero, H. Pastor-Ramírez, L. Álvarez-Amor, J. A. Del Campo, D. Maya-Miles, R. Montero-Vallejo, A. Cárdenas-García, M. J. Pareja and S. Gato-Zambrano, *Sci. Rep.*, 2022, **12**, 3418.
2 J. K. Tan, N. N. M. Salim, G. H. Lim, S. Y. Chia, J. Thumboo and Y. M. Bee, *PLoS One*, 2022, **17**, e0275920.
3 H. Sun, P. Saeedi, S. Karuranga, M. Pinkepank, K. Ogurtsova, B. B. Duncan, C. Stein, A. Basit, J. C. Chan and J. C. Mbanya, *Diabetes Res. Clin. Pract.*, 2022, **183**, 109119.
4 Y. Fu, M. Chen and L. Si, *BMJ Global Health*, 2022, **7**, e007714.
5 A. Fatoni, A. N. Aziz and M. D. Anggraeni, *Sensing and Bio-Sensing Research*, 2020, **28**, 100325.
6 R.-A. Doong and H.-M. Shih, *Biosens. Bioelectron.*, 2010, **25**, 1439–1446.
7 F. F. Franco, R. A. Hogg and L. Manjakkal, *Biosensors*, 2022, **12**, 174.
8 N. Salarizadeh, M. Habibi-Rezaei and S. J. Zargar, *Mater. Chem. Phys.*, 2022, **281**, 125870.
9 K. Babitha, P. Soorya, A. P. Mohamed, R. Rakhi and S. Ananthakumar, *Mater. Adv.*, 2020, **1**, 1939–1951.
10 J. Yoon, Y. S. Yoon and D.-J. Kim, *ACS Appl. Nano Mater.*, 2020, **3**, 7651–7658.
11 Y. Wang, X. Wang, W. Lu, Q. Yuan, Y. Zheng and B. Yao, *Talanta*, 2019, **198**, 86–92.
12 J. Liu, R. Siavash Moakhar, A. Sudalaiyadum Perumal, H. N. Roman, S. Mahshid and S. Wachsmann-Hogiu, *Sci. Rep.*, 2020, **10**, 1–11.
13 X. Chen, S. Zhang, W. Han, Z. Wu, Y. Chen and S. Wang, *J. Chem. Technol. Biotechnol.*, 2018, **93**, 3353–3363.
14 P. Yager, T. Edwards, E. Fu, K. Helton, K. Nelson, M. R. Tam and B. H. Weigl, *Nature*, 2006, **442**, 412–418.
15 M. Thakur, N. Cai, M. Zhang, Y. Teng, A. Chernev, M. Tripathi, Y. Zhao, M. Macha, F. Elharouni, M. Lihter, L. Wen, A. Kis and A. Radenovic, *npj 2D Mater. Appl.*, 2023, **7**, 11.
16 S. Garaj, W. Hubbard, A. Reina, J. Kong, D. Branton and J. A. Golovchenko, *Nature*, 2010, **467**, 190–193.
17 B. Špačková, H. Šípová-Jungová, M. Käll, J. Fritzsche and C. Langhammer, *ACS Sens.*, 2021, **6**, 73–82.
18 Q. Ouyang, L. Tu, Y. Zhang, H. Chen, Y. Fan, Y. Tu, Y. Li and Y. Sun, *Anal. Chem.*, 2020, **92**, 14947–14952.
19 S. He, B. Song, D. Li, C. Zhu, W. Qi, Y. Wen, L. Wang, S. Song, H. Fang and C. Fan, *Adv. Funct. Mater.*, 2010, **20**, 453–459.
20 X. Chen, H. Zhang, R. H. Tunuguntla and A. Noy, *Nano Lett.*, 2019, **19**, 629–634.
21 W. Thunyakontirakun, S. Sriwichai, S. Phanichphant and R. Janmanee, *Mater. Today: Proc.*, 2019, **17**, 2070–2077.
22 X. Leng, S. Chen, K. Yang, M. Chen, M. Shaker, E. E. Vdovin, Q. Ge, K. S. Novoselov and D. V. Andreeva, *Surf. Rev. Lett.*, 2021, **28**, 2140004.
23 K. Yang, M. Chen, Q. Wang, S. Grebenchuk, S. Chen, X. Leng, K. S. Novoselov and D. V. Andreeva, *Adv. Funct. Mater.*, 2022, **32**, 2201904.
24 S. Chortarea, O. C. Kuru, W. Netkueakul, M. Pelin, S. Keshavan, Z. Song, B. Ma, J. Gómes, E. V. Abalos and L. A. V. de Luna, *J. Hazard. Mater.*, 2022, **435**, 129053.
25 A. Ruiz, M. A. Lucherelli, D. Murera, D. Lamon, C. Ménard-Moyon and A. Bianco, *Carbon*, 2020, **170**, 347–360.
26 K. Kostarelos and K. S. Novoselov, *Science*, 2014, **344**, 261–263.
27 K. Kostarelos and K. S. Novoselov, *Nat. Nanotechnol.*, 2014, **9**, 744–745.
28 D. V. Andreeva, M. Trushin, A. Nikitina, M. C. F. Costa, P. V. Cherepanov, M. Holwill, S. Chen, K. Yang, S. W. Chee, U. Mirsaidov, A. H. Castro Neto and K. S. Novoselov, *Nat. Nanotechnol.*, 2021, **16**, 174–180.
29 M. Akram, M. Alam, H. Ji, A. Mahmood, T. Munir, M. Iqbal, M. Saleem, N. Amin and A. Wu, *IOP Conf. Ser.: Mater. Sci. Eng.*, 2019, **474**, 012060.
30 X. Qu, A. Wirsen and A.-C. Albertsson, *Polymer*, 2000, **41**, 4589–4598.
31 C. X. Xie, T. C. Tian, S. T. Yu and L. Li, *J. Appl. Polym. Sci.*, 2019, **136**, 46911.
32 J. Wu, Z.-G. Su and G.-H. Ma, *Int. J. Pharm.*, 2006, **315**, 1–11.
33 J. Ostrowska-Czubenko, M. Gierszewska and M. Pieróg, *J. Polym. Res.*, 2015, **22**, 153.
34 Z. Wang, D. Chen, B. Gu, B. Gao, T. Wang, Q. Guo and G. Wang, *Spectrochim. Acta, Part A*, 2020, **227**, 117671.
35 N. Sohal, B. Maity and S. Basu, *RSC Adv.*, 2021, **11**, 25586–25615.
36 Y. Yan, J. Gong, J. Chen, Z. Zeng, W. Huang, K. Pu, J. Liu and P. Chen, *Adv. Mater.*, 2019, **31**, 1808283.

37 C.-M. Lehr, J. A. Bouwstra, E. H. Schacht and H. E. Junginger, *Int. J. Pharm.*, 1992, **78**, 43–48.
38 X. Chen and A. Noy, *APL Mater.*, 2021, **9**, 020701.
39 X. Strakosas, J. Selberg, P. Pansodtee, N. Yonas, P. Manapongpun, M. Teodorescu and M. Rolandi, *Sci. Rep.*, 2019, **9**, 10844.
40 A. Wiorek, M. Parrilla, M. Cuartero and G. A. Crespo, *Anal. Chem.*, 2020, **92**, 10153–10161.
41 A. I. Visan, G. Popescu-Pelin and G. Socol, *Polymers*, 2021, **13**, 1272.
42 A. Chyzy, M. Tomczykowa and M. E. Plonska-Brzezinska, *Materials*, 2020, **13**, 188.
43 G. Suresh, Y. Samata, P. Naik and V. Kumar, *J Clin Diagn Res*, 2014, **8**, ZC18.
44 L. Tang, S. J. Chang, C.-J. Chen and J.-T. Liu, *Sensors*, 2020, **20**, 6925.